Optical Materials xxx (2014) xxx–xxx

Contents lists available at ScienceDirect

Optical Materials

journal homepage: www.elsevier.com/locate/optmat

Sol–gel synthesis, structural and luminescence properties of MT-doped SiO_2/Zn_2SiO_4 nanocomposites

J. El Ghoul [a,b,*], K. Omri [a], S.A. Gómez-Lopera [c], L. El Mir [a,b]

[a] Laboratoire de Physique des Matériaux et des Nanomatériaux Appliquée à l'Environnement, Faculté des Sciences de Gabès, Cité Erriadh Manara Zrig, 6072 Gabès, Tunisia
[b] Al Imam Mohammad Ibn Saud Islamic University (IMSIU), College of Sciences, Department of Physics, Riyadh 11623, Saudi Arabia
[c] Dep. de Fisica Aplicada, Universidad Politécnica de Cartagena (UPCT), Campus Alfonso XIII, 30203 Cartagena, Spain

ARTICLE INFO

Article history:
Received 19 July 2013
Received in revised form 9 January 2014
Accepted 22 January 2014
Available online xxxx

Keywords:
Zn_2SiO_4
Optical properties
Nanostructures
Photoluminescence
Sol–gel

ABSTRACT

The sol–gel method is used for the preparation of undoped, Mn and V-doped Zn_2SiO_4 particles embedded in SiO_2 host matrix. The phase purity and morphological features were characterized by X-ray diffraction (XRD) and transmission electron microscopy (TEM) investigations. The obtained SiO_2/Zn_2SiO_4 nanocomposite, exhibits a strong photoluminescence (PL) band centered at around 760 nm, attributed to energy transfer occurs from Zn_2SiO_4 particles to NBOHs interfaces defects. In addition, the PL spectrum for the SiO_2/Zn_2SiO_4:Mn nanocomposite showed that a dominant peak at 525 nm appeared, which originated from the $^4T_1$–$^6A_1$ transitions of Mn^{2+} ions. In the case of SiO_2/Zn_2SiO_4:V, the PL reveals a band centered at about 540 nm attributed to the effect of the V^{5+} in the host matrix nanocomposite.

Published by Elsevier B.V.

1. Introduction

In recent years, a great deal of interest has been focused on the fabrication and characterization of zinc orthosilicate (α-Zn_2SiO_4, willemite). Potential fields of application are, for example, optics and optoelectronics, pharmaceutics or biological and medical diagnostics [1–3]. Just like transition metal (TM) doped zinc orthosilicate are highly photostable, exhibit long luminescence lifetimes and narrow emission bands. However, the emission color is dependent on the particle size [4]. It can be adjusted by the choice of the host material and dopants and their combination. The luminescence intensity is dependent on the concentration of doping ions, the crystal structure of the host material, and the degree of crystallinity [5]. The high chemical stability and bright luminescent performance of these nanomaterials make them potentially suitable for biological labeling [3].

Traditionally, this phosphor is prepared by the solid-state reaction method, which involves a pulverizing process and subsequent high-temperature firing. The resulting Zn_2SiO_4:Mn powder phosphors are utilized as paints. However, it is difficult to obtain reliable intensity using such methods, probably because of inhomogeneous distribution of activator ions, phase separation and contamination of impurities. Therefore, recent investigations have addressed development of some alternative synthetic procedures for this phosphor, such as hydrothermal method [6] polymer pyrolysis [7] and sol–gel method [8,9]. Among them the sol–gel method has been confirmed to have more advantages in lowering the firing temperature, distributing the activator ions homogeneously and improving the emission efficiency for the powder phosphors [10,11]. Additionally, the sol–gel technology is suitable for deposition of thin amorphous and crystalline films, which have found extensive applications in many fields [12].

At present, Taghavinia et al. [13] used porous silicon as one of the starting materials and impregnated porous silicon layers with luminescent Zn_2SiO_4:Mn^{2+} particles. Porous silicon was directly involved in the reaction responsible for the formation of luminescent Zn_2SiO_4 phosphors. The phosphor particles were obtained inside a transparent porous body, making it possible to activate porous silicon layers with highly efficient phosphors [13]. Kang and Park used the colloidal solution method to fabricate spherical Zn_2SiO_4 phosphors with an optimal emission intensity that was 112% that of commercially available materials [14]. Although these chemical methods can be applied to produce fine particles with good luminescence, they have the shortcomings related to complex processing, difficulties in achieving controllability and mass production, and high cost [15–17].

In this study, the method is applied to prepare Zn_2SiO_4 (SZ), Zn_2SiO_4:Mn (SZM) and Zn_2SiO_4:V (SZV) particles embedded in

* Corresponding author at: Al Imam Mohammad Ibn Saud Islamic University (IMSIU), College of Sciences, Department of Physics, Riyadh 11623, Saudi Arabia.
E-mail addresses: jaber.elghoul@fsg.rnu.tn, ghoultn@yahoo.fr (J. El Ghoul).

http://dx.doi.org/10.1016/j.optmat.2014.01.019
0925-3467/Published by Elsevier B.V.

silica monolith by the same protocol of sol–gel method combined with a furnace firing [4,18,19] but using for the first time, manganese and vanadium doped zinc oxide nanoparticles and studied the structural and optical properties of the obtained nanocomposites.

2. Experimental

2.1. Preparation

The preparation of colloid suspension particles in silicate host matrix has been done in three steps. In the first one, nanocrystalline ZnO, ZnO:Mn and ZnO:V aerogels were prepared by a sol–gel method under supercritical conditions of ethyl alcohol (EtOH) based on El Ghoul et al. protocol [4,8,9,20], where the water for hydrolysis was slowly released by esterification reaction to control the size of the formed nanoparticles. In the second step, we have prepared ZnO, ZnO:Mn and ZnO:V confined in silica aerogel according to the following process: 0.5 ml of TEOS was first dissolved in EtOH. Then, with constant stirring of the mixture of TEOS and EtOH, 0.44 ml of water and 30 mg of nanoparticles powder prepared in the first step were added. The whole solution was stirred for about 30 min, resulting in the formation of a uniform sol. The sols were transferred to tubes in ultrasonic bath where 100 ml of fluoride acid was added. The wet gel formed in few seconds. Monolithic and white aerogel was obtained by supercritical drying in EtOH as described in the first step. Finally, silica glasses containing SZ, SZM and SZV particles were obtained after firing aerogel at 1200 °C for 2 h.

2.2. Characterizations

The crystalline phases of annealed samples were identified by X-ray diffraction (XRD) using a Bruker D5005 powder X-ray diffractometer using a Cu Kα source (1.5418 Å radiation). Crystallite sizes were estimated from the Scherrer's equation [21].

$$G = \frac{0.9\lambda}{B\cos\theta_B} \quad (1)$$

where λ is the X-ray wavelength (λ = 1.5418 Å), θ_B is the maximum of the Bragg diffraction peak (rad.) and B is the line width at half maximum.

Transmission electron microscopy (TEM, JEM-200CX) was used to study the morphology and particle size of the phosphor powders. The specimens for TEM were prepared by putting the as-grown products in EtOH and immersing them in an ultrasonic bath for 15 min, then dropping a few drops of the resulting suspension containing the synthesized materials onto TEM grid. For photoluminescence (PL) measurements, the 450 W Xenon lamp was used as an excitation source. The emitted light from the sample collected by an optical fiber on the same side as that of excitation was analyzed with a Jobin–Yvon Spectrometer HR460 and a multichannel CCD detector (2000 pixels). The photoluminescence excitation (PLE) measurements were performed on a Jobin–Yvon Fluorolog 3–2 spectrometer. The decays were analyzed by a PM Hamamatsu R928 and a scope Nicolet 400 with a time constant on the order of 1 ns. The low temperature experiments were carried out in a Janis VPF-600 Dewar with variable temperature controlled between 78 and 300 K.

3. Results and discussion

3.1. Structural studies

Fig. 1 shows X-ray diffraction spectra obtained from the SZ (a), SZM (b) and SZV (c) nanocomposites treated at 1200 °C for 2 h in air. These spectra show the X-ray diffraction pattern corresponding to a well-developed willemite structure (α-Zn_2SiO_4, JCPDS No. 37-1485) [8,22]. The lattice constants calculated from the XRD pattern for the three samples are about a = 13.939 Å and c = 9.301 Å, which are very close to willemite α-Zn_2SiO_4 [4,18,23]. The peak signatures of hexagonal wurtzite ZnO were also observed. Therefore, the hexagonal ZnO and willemite Zn_2SiO_4 may coexist in the composite. However, at high temperature, the surface mobility of Zn and Si species is high enough, so they move and diffuse inside the porous body and contribute to the formation of zinc silica phase. The sharpness of the diffraction peaks indicates that the size of the crystalline particles is about 80 nm [8,18]. This result indicates that α-Zn_2SiO_4 has a rhombohedral structure [4]. It is clear that the crystalline phase is the most dominant one corresponding to the α-phase Zn_2SiO_4, in parallel we note the appearance of three other phases that correspond to ZnO, cristobalite and quartz [4]. Therefore, the hexagonal zinc oxide and willemite Zn_2SiO_4 coexist in the composite, this means that the solid reaction at higher temperature is not complete and the obtained composite is formed by very small ZnO nanoparticles covered by willemite Zn_2SiO_4 as a shell supported by SiO_2 as a host matrix. Average grain size (G) of the crystallites Zn_2SiO_4 varies from 50 nm to 80 nm, has been estimated using Scherrer's formula (1). However, Jiang et al. [22] predicted that the particle average size for the Zn_2SiO_4 nanopowder was 100 nm.

The TEM micrographs, HRTEM image and EDX analyzes of the SiO_2/Zn_2SiO_4 nanocomposites treated at 1200 °C for 2 h in air are shown in Fig. 2. The morphology of the sample is found to be nearly spherical in nature with the diameters ranging from 40 to 90 nm. It clearly shows that the average particle size is nanoscale and it is in accordance with the results of the XRD.

EDX analysis showed the presence of the elements Zn and Si. At high temperature at 1200 °C, Zn and Si species, move and diffuse inside the porous body to form Zn_2SiO_4 phase. In parallel, the HRTM image and the corresponding EDX analysis showed the presence of nanoparticles that correspond to ZnO in sample, such results is confirmed that the results obtained by XRD.

The TEM images corresponding to SZM (Fig. 3a) and SZV (Fig. 3b). The Zn_2SiO_4 colloid suspension is formed in silica host matrix with a particle size of about 70 nm. The EDX spectrum of the doped sample showed signals directly related to the dopants. Zn, Si and O appeared as the main components with low levels of Mn and V (Fig. 3). This confirmed the formation of SZM and SZV phases.

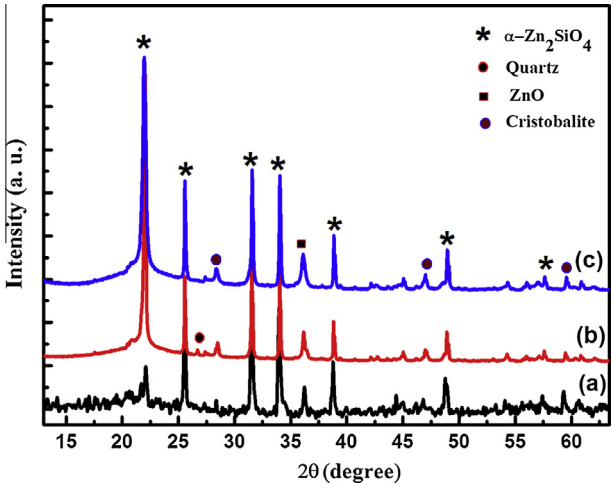

Fig. 1. X-ray diffraction pattern of the (a) Zn_2SiO_4, (b) Zn_2SiO_4:Mn and (c) Zn_2SiO_4:V nanocomposite.

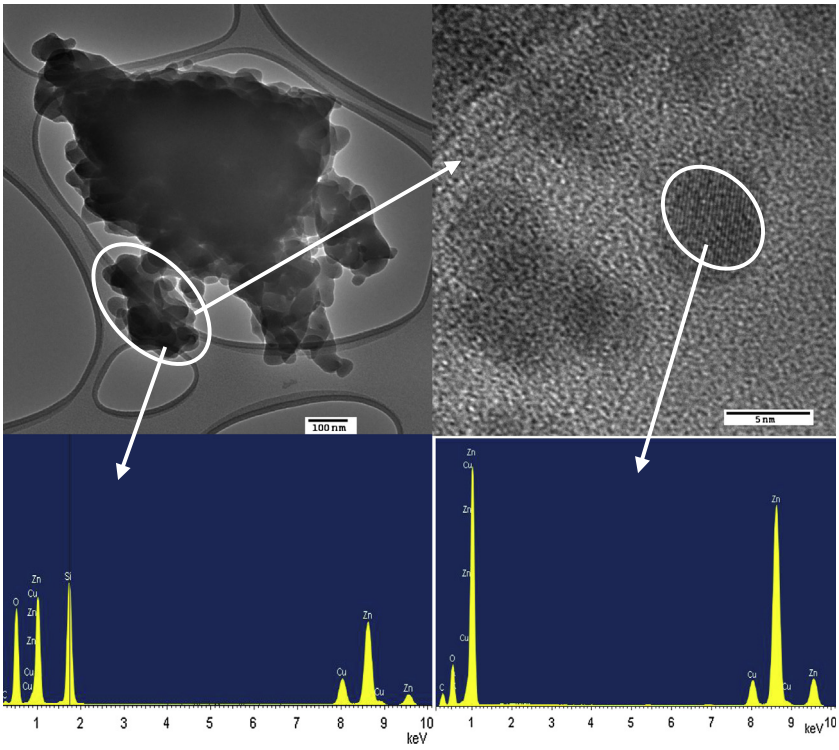

Fig. 2. TEM photograph showing the general morphology of the Zn_2SiO_4 nanocomposite and its EDX analysis.

3.2. Optical studies

3.2.1. Photoluminescence property

We used the excitation wavelength 245 nm to measure the photoluminescence (PL) spectra of SZ nanocomposite at different temperatures. As shown in Fig. 4, the sample has broad PL bands centered at different positions. A strong near-UV emission located at about 400 nm has been observed. This emission, different from what is usually seen, could be attributed to the exciton-related emission of ZnO near the band edge [24]. The striking feature is the absence of almost any of the usually reported visible emission bands in the range 400–650 nm (2.4–2.7 eV), and the appearance of a strong and wide near infrared (NIR) emission band centered around 760 nm, besides a near band edge emission including the bound exciton line [8]. As illustrated in Fig. 5, the photoluminescence emission spectra of SZM nanocomposites at different temperatures. The green emission has been assigned to an electronic transition of $^4T_1(^4G) \rightarrow {}^6A_1(^6S)$ peaking at the wavelength 525 nm and which is a parity forbidden emission transition of Mn^{2+} ions [25]. The graph shows that the relative PL intensity of

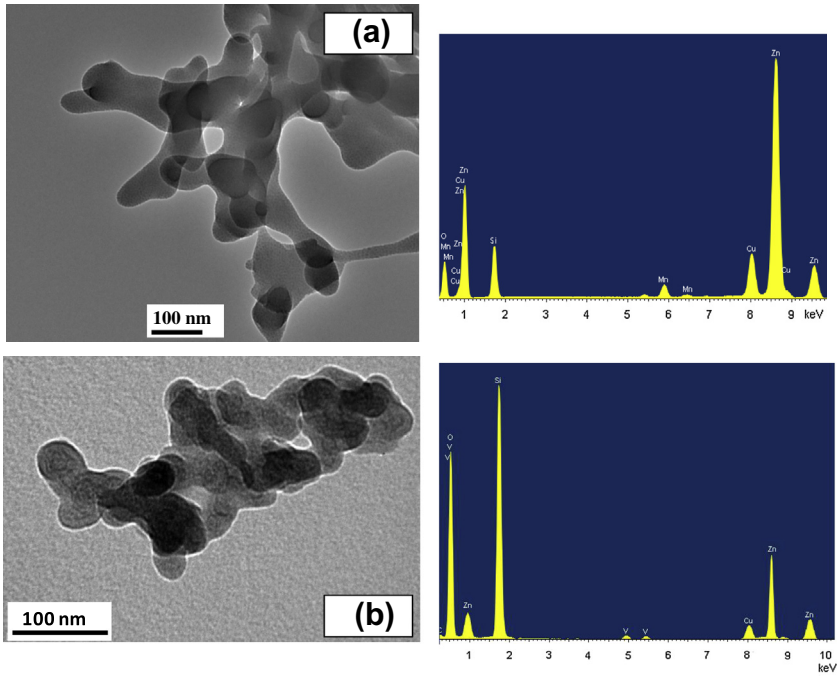

Fig. 3. TEM photograph showing the general morphology of the (a) Zn_2SiO_4:Mn and (b) Zn_2SiO_4:V nanocomposite and its EDX analysis.

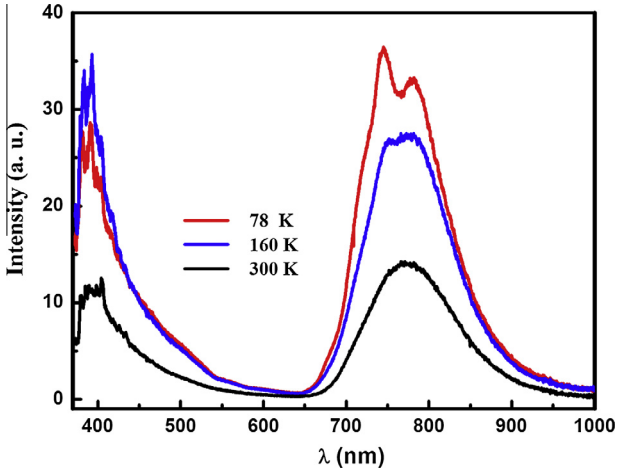

Fig. 4. PL spectra of the Zn_2SiO_4 nanocomposite at different temperatures.

the nanocomposites decreases as the measured temperature increases. It is generally recognized that the luminescence of the Mn^{2+} ion depends on the Zn_2SiO_4 host crystal field. Mn^{2+} ions in the Zn_2SiO_4 host with higher crystallinity feel a stronger crystal field. Increasing the crystal field reduces the energy difference of the ground and first excited state, resulting in peak broadening and red-shift of the emission peak [26]. This emission centered at 525 nm, corresponds to the d–d transition of Mn^{2+} through energy transfer from Zn_2SiO_4 [27,28]. With Mn^{2+} occupies part of the Zn^{2+} sites, which is coordinated by four oxygen atoms [25]. The weak crystal field around Mn^{2+} results in the low splitting width of its 3d energy levels, in accordance with the observations of Stevels and Vink [29].

The PL spectrum of the SiO_2/Zn_2SiO_4:V nanocomposite obtained by the 290 nm excitation wavelength consists on a very intensive emission band located in the green–yellow spectral range. Fig. 6 shows the PL spectra of the SiO_2/Zn_2SiO_4:V nanocomposite measured in the 400–900 nm wavelength range at different temperatures. The intensity of the luminescence band observed at 540 nm decreases as the temperature increases. The shape and the energy location of the PL emission bands are characteristic for a deep levels emission. In fact; it is well understood that the surface of silica is quite easily contaminated by water vapor resulting in silanol-related chemical bonds, such as Si–OH. We propose that the ground electronic state for different kinds of OH-related species is the same, despite the variation in excited electronic states. Therefore, the electronic transitions for all kinds of PL centres involve the Si–OH vibration in the ground state of the water-like species, but the relative intensity of different components depends strongly on measurement temperature [30]. In our previous works, using the same protocol, we have seen a similar behavior after incorporation of Al_2O_3 in silica but not with the incorporation of ZnO in silica [30]. This result is in agreement with the studies of Dzwigaj and Michel Che [31], i.e., that the vanadium-related species surrounded by silanol groups improve the luminescence intensity of these broad emission bands in the visible range. Generally in inorganic oxide matrices, vanadium is usually present in three different oxidation states, V^{3+} ($3d^2$), V^{4+} ($3d^1$)and V^{5+} ($3d^0$), where by the trivalent ion is readily oxidized to higher valence [32,33]. We join the opinion which asserts that the PL band is attributed to the presence of V^{5+} ions and covers a broad band ranging from 400 to 700 nm [5,31,33,34]. We notice also the presence of nine very broad emission bands appear between 1.80 and 2.76 eV with vibrational progressing of $\Delta\gamma = 960\ cm^{-1}$. These bands have been attributed to Si–OH vibration on the surface [30], but we suggest that this phenomenon corresponds to the transitions from the lowest vibrational level of the excited triplet state $T_1(V^{4+} - O^-)$ to the various vibration levels of the ground state $S_0(V^{5+} = O^{2-})$ [35].

3.2.2. Photoluminescence excitation (PLE)

Photoluminescence excitation (PLE) spectra of the SZ, SZM and SZV nanocomposites at the measurement temperature $T = 78$ K are displayed in Fig. 7. In the case of SZ nanocomposite (Fig. 7a), the PLE spectrum detected at 760 nm which shows the appearance of a very weak peak at 375 nm (3.3 eV) relative to its value at higher energy. The low energy excitation band is due to carrier excitation in the near band edge of ZnO nanoparticles. Indeed, as it has been shown by Chakrabarti et al. [36], a high annealing temperature (1073 K) results in a rapid grain growth and when the radii of the nanoparticles increases to 8.2 nm, a bulk ZnO like band gap is obtained. However, the most efficient excitation process is with photon energies of about 5.4 eV (230 nm), which are much higher than the ZnO bulk band gap. Unfortunately, the high energy peak position of the PLE spectrum cannot be clearly determined due to the high energy range limit of our setup.

The shape and the structured nature of the PL emission band, the large shift between the PL and the PLE energy peaks of the 760 nm PL emission are in principle a signature of a deep level emission with an electron–phonon coupling. However, its full width at half maximum (FWHM) dependence with temperature

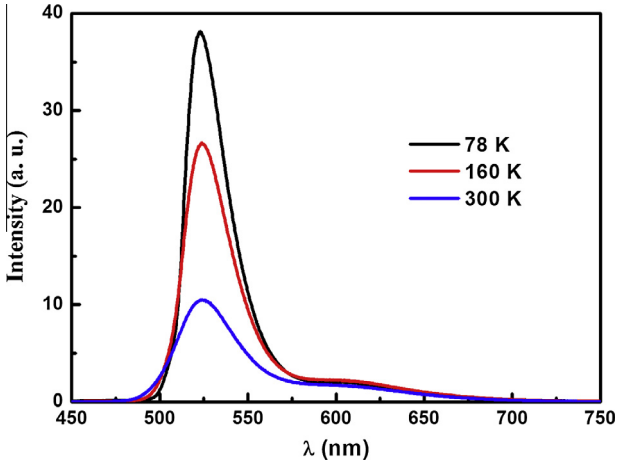

Fig. 5. PL spectra of the Zn_2SiO_4:Mn nanocomposite at different temperatures.

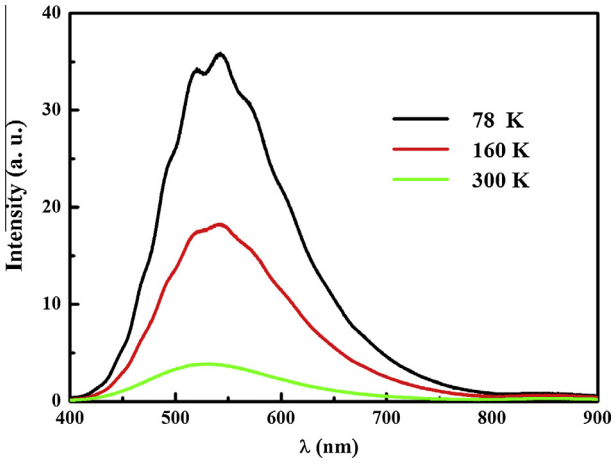

Fig. 6. PL spectra of the Zn_2SiO_4:V nanocomposite at different temperatures.

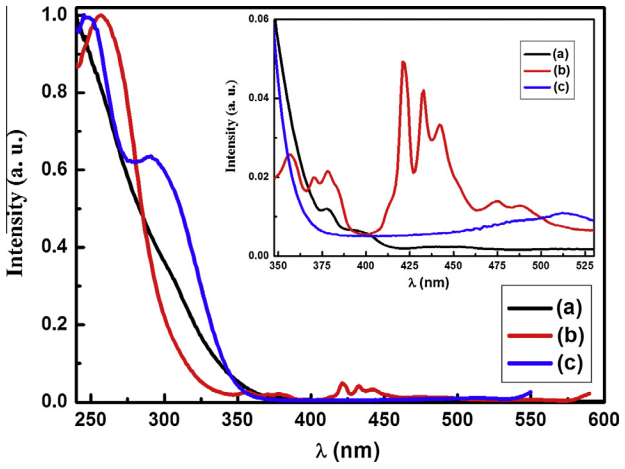

Fig. 7. PLE spectra of the (a) Zn_2SiO_4, (b) Zn_2SiO_4:Mn and (c) Zn_2SiO_4:V nanocomposite.

cannot be fitted according to this model, which rules out the hypothesis of an electron–phonon coupling. One should also consider the possible connection of the ZnO/Zn_2SiO_4 and Zn_2SiO_4/SiO_2 interface states with the observed emission band. Indeed, it has been demonstrated that Si–O–Zn bonds can be formed in sol–gel ZnO/SiO_2 composites [8], resulting in the creation of interface states. But, as it has been explained by Fu et al. [37], the Zn–O–Si interface state is shallow as compared to V_O or Zn_i related states. As a consequence, these interface states could not be involved in our NIR emission band, but they are involved in the observed UV emission band. The absence of the commonly reported green–yellow emission band can be explained by the fact that, during high temperature annealing in air, oxidation process should take place. As a result oxygen is incorporated in interface sites and should therefore induce a large decrease in intensity of the OH-related PL emission. From the analysis of the PL and PLE spectra, it can be concluded that the excitation peak near 760 nm can be attributed with the formation of NBOHs excited at the spectral region $h\nu \geqslant 5.4$ eV, such band arises from the absorption of Zn_2SiO_4 particles. This suggests that an energy transfer occurs from Zn_2SiO_4 particles to NBOHs interface defects [38]. PLE spectra, in the case of the SiO_2/Zn_2SiO_4:Mn nanocomposites of the band detected at 525 nm, show a strong excitation band ranging from 240 to 300 nm with a maximum at about 255 nm (4.9 eV) compared to bands in UV–vis range (Fig. 7b). The band at 255 nm is considered to be responsible for the emission at 525 nm. The spectra fully agree with previously measured excitation spectrum of Zn_2SiO_4:-Mn [39]. The broad excitation peak at 255 nm could be attributed to a charge transfer transition (or the ionization of manganese) from the divalent manganese ground state (Mn^{2+}) to the conduction band (CB) [25,40]. In addition to the CT band, other bands (inset) of Mn^{2+} (d–d) transitions are also observed at higher wavelengths (350–500 nm), these are caused by crystal field splitting of the ^4D and ^4G levels as shown by the Orgel diagram for Mn^{2+} [8,39]. The electrons in the $^6A_1$ (^6S) ground state of Mn^{2+} ions, are excited to the conduction band of Zn_2SiO_4 by photons, and the free electrons in the conduction band relax back to the $^4T_1$ (^4G) excited state through a non-radiative process [39]. Finally, this is followed by a radiative transition from the $^4T_1$ (^4G) excited state to the $^6A_1$ (^6S) ground state, giving rise to a green emission band (525 nm). On the other hand, the PLE spectra of the SiO_2/Zn_2SiO_4:V nanocomposite detected at 540 nm are given in Fig. 7c. These results, observed for the first time, show an excitation band ranging from 240 to 350 nm with a maximum at about 250 nm. This excitation band was attributed to the charge transfer (CT) in Zn_2SiO_4 lattice [8,24]. The second peak excitation at about 300 nm is related to the charge transfer in groups of vanadyl. This mechanism is strongly affected by the ligand field strength may be understood as an energy transfer process from O^{2-} to V^{5+} which occurs intrinsically in the vanadyl group [34]. The width of the PLE band prove that there are various origins of the luminescent centres and the nature of these bands is not completely well established and calls for further investigations. The large shift between the PL and PLE energy peaks, the shape and the structured nature of the PL emission bands are very close to those of hydroxyl-related species [34] with small shift, probably due to the change of the environment.

4. Conclusion

In conclusion, luminescent nanocomposites of undoped, Mn and V doped Zn_2SiO_4 in a silica matrix were synthesized by sol–gel method. The X-ray diffraction and TEM of our nanocomposites show a crystalline phase with a particle size ranging between 50 and 90 nm. The PL spectra of the SZ, SZM and SZV nanocomposites show a strong near-infrared luminescence band and the absence of the commonly reported visible emission bands, a dominant peak at 525 nm and a band centered at 540 nm, respectively. Based on the analysis of the PL and PLE spectra of this sample, it can be concluded that the luminescence bands can be attributed to energy transfer which occurs from Zn_2SiO_4 particles to NBOHs interfaces defects, Mn^{2+} in Zn_2SiO_4 particle and the presence of V^{5+} ions, respectively. Our results highlight the importance of temperature of synthesis and dopant concentration of the material whose objective is to increase the life of components and prevent contamination caused by the external environment. Furthermore, no change in the PL spectra, either in shape or position, was observed, even after being aged for a long period of time, indicating the time stability of the composite material. This result strongly suggests that the production of nanoparticles in SiO_2 matrix by sol–gel is a simple way to maintain the luminescence spectra of the nanoparticles. In this regard, time-resolved luminescence studies are essential to unraveling the origin of the observed quenching behavior.

References

[1] H. Chander, Mater. Sci. Eng., R 49 (2005) 113–155.
[2] H.A. Höppe, Angew. Chem. Int. Ed. 48 (2009) 3572–3582.
[3] J. Shen, L.D. Sun, C.H. Yan, Dalton Trans. 42 (2008) 5687–5697.
[4] K. Omri, J. El Ghoul, A. Alyamani, C. Barthou, L. El Mir, Physica E 53 (2013) 48–54.
[5] J. El Ghoul, K. Omri, L. El Mir, C. Barthou, S. Alaya, J. Lumin. 132 (2012) 2288–2292.
[6] Q.H. Li, S. Komarnen, R. Roy, J. Mater. Sci. 30 (1995) 2358–2364.
[7] K. Su, D.T. Tilley, M.J. Sailor, J. Am. Chem. Soc. 118 (1996) 3459–3468.
[8] J. El Ghoul, K. Omri, A. Alyamani, C. Barthou, L. El Mir, J. Lumin. 138 (2013) 218–222.
[9] J. El Ghoul, C. Barthou, M. Saadoun, L. El Mir, J. Phys. B 405 (2010) 597–601.
[10] Q. Lu, G. Yun, Ceram. Int. 39 (2013) 3533–3538.
[11] J. Lin, Q. Su, J. Mater. Chem. 5 (1995) 603–606.
[12] W.C. Wang, Y.T. Tian, K. Li, E.Y. Lu, D.S. Gong, X.J. Li, Appl. Surf. Sci. 273 (2013) 372–377.
[13] N. Taghavinia, G. Lerondel, H. Makino, A. Parisini, A. Yamamoto, T. Yao, Y. Kawazoe, T. Goto, J. Lumin. 96 (2002) 171–175.
[14] E.S. Park, T.H. Cho, H.J. Chang, Appl. Chem. 1 (1997) 406–409.
[15] M. Abdullah, S. Shibamoto, K. Okuyama, Opt. Mater. 26 (2004) 95–100.
[16] T.H. Cho, H.J. Chang, Ceram. Int. 29 (2003) 611–618.
[17] A. Shila, D.G. Jeannette, C. Brigitte, Mater. Res. Bull. 43 (2008) 2751–2762.
[18] T.I. Thristov, N.V. Popovich, S.S. Galaktionov, N.P. Soshchin, Inorg. Mater. 32 (1996) 80–84.
[19] R. Morimo, R. Monchinaga, K. Nakamura, Mater. Res. Bull. 29 (1994) 751–756.
[20] J. El Ghoul, C. Barthou, L. El Mir, Physica E 44 (2012) 1910–1915.
[21] B.D. Cullity, Elements of X-ray Diffractions, Addison-Wesley, Reading, MA, 1978. 102.
[22] Y. Jiang, J. Chen, Z. Xie, L. Zheng, J. Mater. Chem. Phys. 120 (2010) 313–318.
[23] M. Takesue, H. Hayashi, R. Lee Smith Jr., J. Prog. Cryst. Growth Charact. Mater. 55 (2009) 98–124.

[24] J. El Ghoul, C. Barthou, M. Saadoun, L. El Mir, J. Phys. Chem. Solids 71 (2010) 194–198.
[25] R. Selomulya, S. Ski, K. Pita, C.H. Kam, Q.Y. Zhang, S. Buddhudu, J. Mater. Sci. Eng., B 100 (2003) 136–141.
[26] P. Thiyagarajan, M. Kottaisamy, M.S. Ramachandra Rao, Scripta Mater. 57 (2007) 433–436.
[27] X. Li, F. Chen, Mater. Res. Bull. 48 (2013) 2304–2307.
[28] N. Taghavinia, G. Lerondela, H. Makino, A. Yamamoto, T. Yao, Y. Kawazoe, T. Goto, J. Nanotechnol. 12 (2001) 547–551.
[29] A.L.N. Stevels, A.T. Vink, J. Lumin. 8 (1974) 443–446.
[30] L. El Mir, A. Amlouk, C. Barthou, J. Phys. Chem. Solids 67 (2006) 2395–2399.
[31] S. Dzwigaj, M. Michel Che, J. Phys. Chem. B 109 (2005) 22167–22174.
[32] L. El Mir, J. El Ghoul, S. Alaya, M. Ben Salem, C. Barthou, H.J. Von Bardeleben, Physica B 403 (2008) 1770–1774.
[33] M. Morita, S. Kajiyama, T. Kai, D. Rau, T. Sakurai, J. Lumin. 94–95 (2001) 91–95.
[34] G. Gao, R. Meszaros, M. Peng, L. Wondraczek, Opt. Express 19 (2011) A312–A318.
[35] M. Anpo, S. Higashimoto, M. Matsuoka, N. Zhanpeisov, Y. Shioya, S. Dzwigaj, M. Che, Catal. Today 78 (2003) 211–217.
[36] S. Chakrabarti, D. Das, D. Ganguli, S. Chaudhuri, Thin Solid Films 441 (2003) 228–237.
[37] Z. Fu, B. Yang, L. Li, W. Dong, C. Jia, W. Wu, J. Phys.: Condens. Matter 15 (2003) 2867–2872.
[38] L. El Mir, A. Amlouk, C. Barthou, S. Alaya, Physica B 388 (2007) 412–417.
[39] L.E. Orgel, J. Chem. Phys. 23 (1955) 1819–1823.
[40] L. Xiong, J. Shi, J. Gu, L. Li, W. Huang, J. Gao, M. Ruan, J. Phys. Chem. B 109 (2005) 731–736.

Please cite this article in press as: J. El Ghoul et al., Opt. Mater. (2014), http://dx.doi.org/10.1016/j.optmat.2014.01.019